BNL-221092-2021-JAAM

Thickness-Dependent Ordering Kinetics in Cylindrical Block Copolymer/Homopolymer Ternary Blends. Macromolecules

G. S. Doerk, R. Li

To be published in "MACROMOLECULES"

December 2018

Photon Sciences

Brookhaven National Laboratory

U.S. Department of Energy

USDOE Office of Science (SC), Basic Energy Sciences (BES) (SC-22)

DISCLAIMER

Thickness-Dependent Ordering Kinetics in Cylindrical Block Copolymer/Homopolymer Ternary Blends

Gregory S. Doerk,*[,†] Ruipeng Li,[‡] Masafumi Fukuto,[‡] Alfredo Rodriguez,[§] and Kevin G. Yager[†]

[†]Center for Functional Nanomaterials and [‡]National Synchrotron Light Source II, Brookhaven National Laboratory, Upton, New York 11973, United States

[§]Department of Mechanical Engineering, City College of City University of New York, New York, New York 10031, United States

ABSTRACT: The slow kinetics of block copolymer self-assembly may hinder, or even prevent, the realization of expected equilibrium ordered morphologies. Here we investigate the self-assembly kinetics of cylinder-forming polystyrene-*block*-poly(methyl methacrylate) (PS-*b*-PMMA) and its corresponding ternary blends with low molecular weight PS and PMMA in thin films ranging from <1 to several cylinder layers in thickness. *In situ* grazing-incidence X-ray scattering coupled with *ex situ* electron microscopy reveals pathway-dependent ordering substantially altered by homopolymer blending. In particular, the neat (unblended) block copolymer (BCP) is kinetically frustrated in films more than ∼1 cylinder layer thick and is unable to reach a state of ordered hexagonally packed cylinders during the annealing interval. On the other hand, while blends exhibit similar pattern coarsening behavior to neat BCPs for hexagonally ordered cylinders, reorientation transitions between vertical or horizontal cylinders are dramatically accelerated in blend thin films. We infer that more rapid early stage ordering observed in blends can be attributed in part to faster reorientation transitions.

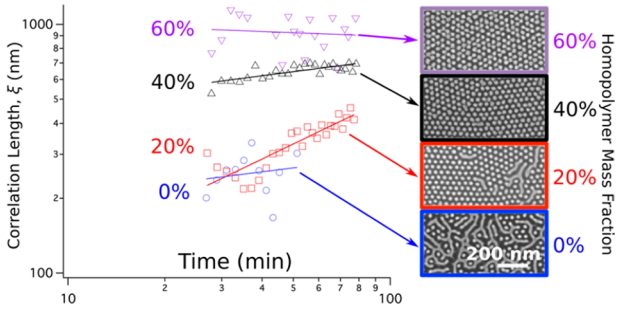

INTRODUCTION

Block copolymers (BCPs) are a class of soft materials well-known to self-assemble to form various nanoscale morphologies (spheres, lamellae, cylinders, etc.) based on the microphase separation of the covalently bound constituent polymer blocks.[1] Thin films of block copolymers that form cylinder domains oriented vertically with respect to the supporting substrate have been used for a variety of applications including nanopatterning,[2] surface nanotexturing for wettability control,[3] and light management[4,5] and for the fabrication of nano-/ultrafiltration membranes.[6−8] Polystyrene-*block*-poly(methyl methacrylate) (PS-*b*-PMMA) is attractive for these applications as it has near equal surface energies at temperatures typically used for thermal annealing (∼200−250 °C),[9] which promotes facile vertical cylinder orientation.

Nevertheless, the ability of cylinders in PS-*b*-PMMA films to orient perpendicularly to an underlying substrate is not assured and depends on factors like surface chemistry,[10−12] film thickness,[10,12−15] annealing temperature,[12,13] and process history.[16−19] The successful formation of BCP domains that span the entire film thickness with minimal defectivity depends crucially on the BCP ordering kinetics. This becomes particularly evident in the self-assembly of vertically oriented cylinders in thicker BCP films (>1 cylinder monolayer),[13,15] which are critical for patterning applications or for membrane fabrication; optimizing self-assembly kinetics is therefore vital to the successful implementation of cylinder-forming block copolymers for various applications.

Recently, we have demonstrated that blending lamellae-forming PS-*b*-PMMA with low molecular weight PS and PMMA homopolymers can dramatically improve ordering kinetics.[20] Here we investigate how low molecular weight homopolymer blending impacts the domain size, orientation, and ordering kinetics for cylinder-forming PS-*b*-PMMA from submonolayer thick films to films with thicknesses more than ∼3 cylinder layers. *In situ* grazing incidence small-angle X-ray scattering (GISAXS) is used to probe these parameters during thermal annealing. The GISAXS investigations are coupled with electron microscopy using selective infiltration of PMMA domains with alumina to "stain" them for a more direct means of characterizing domain morphology and orientation. Using these techniques, we demonstrate that blending dramatically enhances the kinetics of reorientation transitions (e.g., from horizontal to vertical cylinders), which in turn has important implications in early stage self-assembly kinetics.

terminated random copolymer brush to their surfaces according to the method we have described previously.[20] Briefly, a hydroxyl-terminated random copolymer brush of PS and PMMA provided by the Dow Chemical Company (PS-*r*-PMMA-OH; 69% styrene, determined by ^{13}C NMR) was diluted to 1% (w/w) in propylene glycol monomethyl ether acetate (PGMEA) and spun onto 100 mm Si wafers at 1500 rpm. The wafers were baked at 250 °C for 5 min in a nitrogen-enriched environment to promote grafting of the brush to the substrate, followed by rinsing in PGMEA at 3000 rpm to remove ungrafted brush polymer. Cylinder-forming 67 kg/mol PS-*b*-PMMA (M_n = 46-*b*-21 kg/mol; PDI = 1.09), PS homopolymer (M_n = 3.5 kg/mol), and PMMA homopolymer (M_n = 3 kg/mol) were obtained from Polymer Source and used as received. Homopolymers were blended in a weight proportion of PMMA:PS = 3:7 to ensure that the cylinder morphology was maintained across all blend compositions. All solutions were prepared using toluene (Sigma-Aldrich) at a concentration of 1% (w/w). Polymer films were deposited by blade casting using a custom-built tool (100 μm blade−substrate gap, 50 μL solution) in consecutive 10 mm sweeps at speeds of 5, 10, 20, 30, and 45 mm/s. As a result, each sample contains precisely the same polymer film composition, with five different thicknesses. Film thicknesses were measured by optical reflectometry (Filmetrics F20). Some samples were annealed in a vacuum oven at 200 °C.

Grazing-Incidence Small-Angle X-ray Scattering (GISAXS). Synchrotron GISAXS experiments were performed at the 11-BM Complex Materials Science (CMS) beamline of the National Synchrotron Light Source II (NSLS-II) at Brookhaven National Laboratory. Two-dimensional scattering images were collected using a photon-counting area detector (Dectris Pilatus 2M) placed 5.09 m from the sample. Samples were mounted on a custom heater stage and measured under vacuum using an X-ray beam of 13.5 keV (λ = 0.0918 nm). GISAXS data were collected using a 5 s integration time and a grazing-incidence angle of 0.11°. Silver behenate powder was used as a standard for data conversion to q-space. The X-ray beam width was 200 μm (horizontal), illuminating a sample area of ∼5 mm^2. Alignment was performed at 90 °C, 140 °C, and the annealing temperature (200 or 220 °C) to account for the thermal expansion of the stage after ramping from room temperature. Analysis of self-assembly kinetics was limited to isothermal measurements collected at the annealing temperature, but the data sets including the period of the temperature ramp for the curves presented in the text are provided in the Supporting Information (Figures S3 and S7). Two samples were mounted on the *in situ* heating stage for each annealing experiment. The stage cycled through all constant film thickness regions of a sample during measurement to ensure that all measurements were performed over the same approximate annealing time interval. Within a constant film thickness region, the sample was translated by 0.1 mm between consecutive measurements, each ∼2 min apart, to prevent X-ray beam damage effects (e.g., cross-linking).[21] Measurements were performed in the approximate center of each constant film thickness region, and fewer than 40 measurements were performed in each region to avoid the unavoidable thickness gradients that occur within ∼2 mm at the beginning and end of each constant thickness region as a result of acceleration/deceleration of the blade coating stage.

GISAXS analysis was performed using the Python programming environment and SciAnalysis scripts.[22] Structural information was extracted from two-dimensional GISAXS scattering images by taking a line cut along the in-plane direction (q_x, scattering vector normal to the plane of incidence) through the first-order scattering peak. The peak center position (q_x), width (Δq), and integrated intensity were determined using a Gaussian fitting function with a power-law background to account for diffuse scattering. The hexagonal lattice period (i.e., spacing between rows of cylinders), L_0, was determined using $L_0 = 2\pi/q_x$. For horizontally oriented cylinders, the line cut was taken through the first peak above the Yoneda, where $2\pi/q_x$ corresponds to the cylinder−cylinder distance (d), where $d = 2L_0/\sqrt{3}$. The average in-plane correlation length ("grain size"), ξ, was estimated using a Scherrer peak width analysis applied to Δq, after accounting for peak broadening contributions from instrumental and grazing-incidence aspects.[23] Error bars in this work represent one standard deviation (1σ) due to uncertainty in the fit unless noted otherwise. Where scattering peaks for both horizontal and vertical cylinders were observed, a line cut through both peaks was chosen, in which the peak at smaller q_x is attributed to horizontally oriented cylinders. The fraction of horizontal cylinders was estimated based on the ratio between the integrated intensity for the horizontal cylinders and the sum of integrated intensities for both peaks, acknowledging there may be small errors in this estimate based on differences in exit angles, reciprocal space volume, and number of diffraction peaks averaged for the two observed GISAXS peaks.[24] Nevertheless, these absolute errors are not expected to significantly affect the validity of kinetic parameters determined based on analysis of the relative temporal behavior of the two peaks.

Electron Microscopy. After GISAXS measurements, but prior to scanning electron microscopy imaging, samples were infiltrated with alumina via sequential infiltration synthesis[25] (SIS) as described previously.[3,26] Briefly, SIS was performed using four cycles of exposure to trimethylaluminum and water vapor (300 s each) at 85 °C in a commercial atomic layer deposition tool (Cambridge Ultratech Savannah S100) with a base pressure of <3 Torr. Samples were cleaved for cross-sectional imaging, and then a portion of the polymer was removed by O_2 plasma ashing (March Plasma CS1701F, 100 mTorr, 20 W, 60 s) to reveal alumina replicas of the self-assembled structure. Imaging was performed using a Hitachi S-4800 scanning electron microscope at a 5 kV accelerating voltage.

RESULTS AND DISCUSSION

Submonolayer Films. On surfaces that have been chemically functionalized to be nominally "neutral" (i.e., nonpreferential for both the PMMA cylinder and PS matrix phases), vertical domain orientation occurs most readily when the film thickness is less than the hexagonal lattice period (L_0) due to packing frustration for cylinders oriented parallel with the substrate.[10] Therefore, the sub-L_0 thickness regime merits special attention in the investigation cylinder-forming ternary BCP/homopolymer blends for its potential use in nanopatterning applications. Figure 1a shows a plan-view scanning electron micrograph (SEM) of an ∼0.9L_0 thick film of a 67 kg/mol PS-*b*-PMMA cylinder-forming BCP annealed for >1 h at 200 °C to promote self-assembly. To improve imaging contrast, samples were "stained" by infiltration synthesis, an ALD-like process in which a vapor-phase organometallic

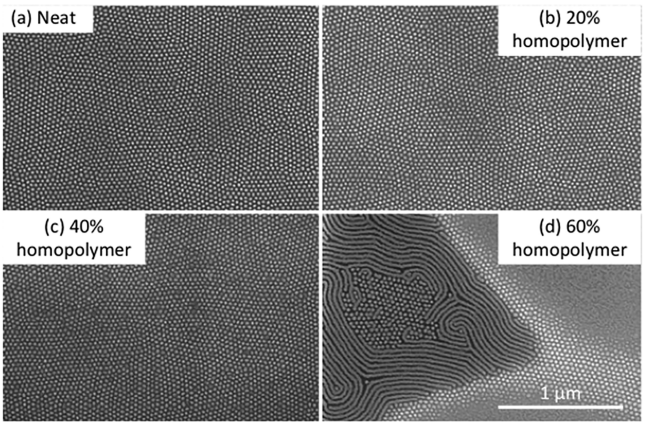

Figure 1. Plan-view SEMs of self-assembled vertically oriented cylinders after annealing at 200 °C for 1 h in submonolayer (0.9−1.0L_0) films using (a) neat BCP and ternary blends with homopolymer mass fractions of (b) 20%, (c) 40%, and (d) 60%. All images are at the same magnification.

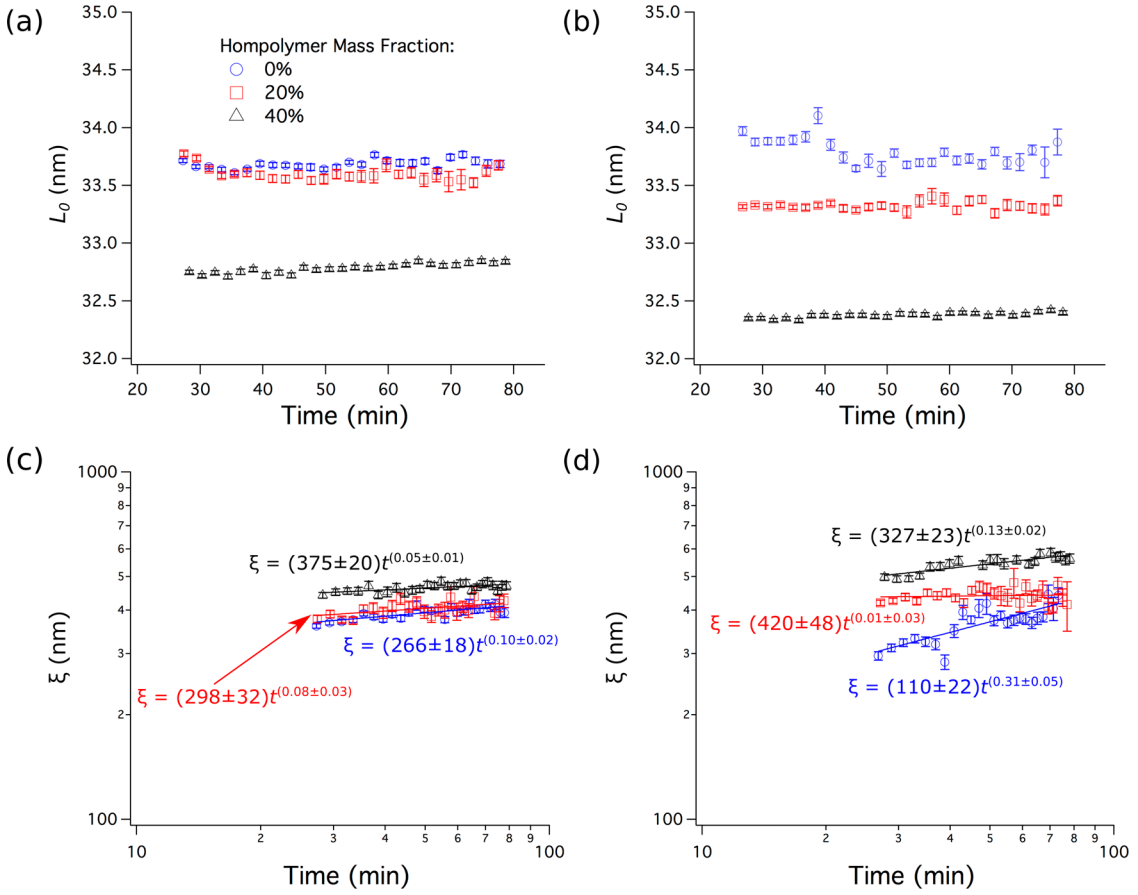

Figure 2. *In situ* GISAXS measurements of dimensional scaling and ordering in neat and ternary blend submonolayer films ($0.9-1.0L_0$) during thermal annealing. The lattice period (L_0) as a function of annealing time at (a) 200 °C and (b) 220 °C. Correlation length (ξ) as a function of annealing time at (c) 200 °C and (d) 220 °C. Solid lines in (c) and (d) are power law fits to the data. The legend in (a) applies to all graphs.

precursor forms a metal oxide (in this case Al_2O_3) selectively within the PMMA domains.[3,20,26] Contrast was further enhanced by partially etching the polymer away using oxygen-based reactive ion etching (see the Experimental Section). Accompanying the SEM of the neat BCP in Figure 1a are SEMs of ternary blend thin films (~$0.9-1.0L_0$ thick) of the same BCP with 3 kg/mol PMMA and 3.5 kg/mol PS homopolymers in a ~3:7 ratio of the two homopolymers to preserve the cylinder morphology. Figures 1b and 1c show SEMs of thin films containing 20% and 40% homopolymer (w/w), respectively. Based on the SEMs alone, the level of order looks comparable. However, when the homopolymer mass fraction is increased to 60% (Figure 1d) dewetting occurs, resulting in the coexistence of a wetting layer, vertical cylinders, or horizontal cylinders depending on the restructured film thickness according to commensurability criteria.[27] Similar results are observed in SEMs of films with approximately the same thickness and homopolymer mass fractions annealed at 220 °C (see Supporting Information Figure S1). Increasing the homopolymer mass fraction to 70% led to increasingly severe dewetting, and a diminished degree of topological order was observed for a 80% homopolymer mass fraction, indicating a gradual transition to a disordered phase beginning with homopolymer mass fractions from 70% to 80% (see Figure S2, where it is noted that the initial film thickness was above a monolayer at ~$1.3L_0$).

GISAXS was used to quantify structural order *in situ* during thermal annealing. L_0 was extracted from Gaussian fits of the first-order scattering peak taken from a line cut along the scattering vector normal to the plane-of-incidence, q_x, according to the relationship that $L_0 = 2\pi/q_x$. The L_0 values measured *in situ* during annealing at 200 and 220 °C for the neat BCP and blends containing 20% and 40% homopolymer are plotted versus annealing time in Figures 2a and 2b, respectively (60% homopolymer blends are excluded based on dewetting). The values of L_0 are reasonably stable during annealing for either temperature. However, the mean L_0 value clearly decreases with increasing homopolymer mass fraction.

This behavior can be understood in light of the much smaller molecular weight of the homopolymer with respect to the BCP ($M_{n,homopolymer}/M_{n,BCP} \approx 0.05$). In these cases, each homopolymer distributes more uniformly within its respective domain to maximize translational entropy, thereby interpenetrating or "wetting" that polymeric block (often termed the "wet brush" regime). The uniform distribution of homopolymer extends to the domain interface, where this interpenetration increases the interfacial area per BCP chain, resulting in relaxation of the BCP chain and a net contraction of the domain spacing.[28]

Interestingly, the same homopolymers paired with a lamellae-forming PS-*b*-PMMA BCP of similar molecular weight (74 kg/mol) to the one used in this report did not result in significant domain contraction.[20] This discrepancy in the domain spacing of lamellar and cylindrical BCPs of comparable molecular weight in response to homopolymer blending is somewhat surprising given that the same chain

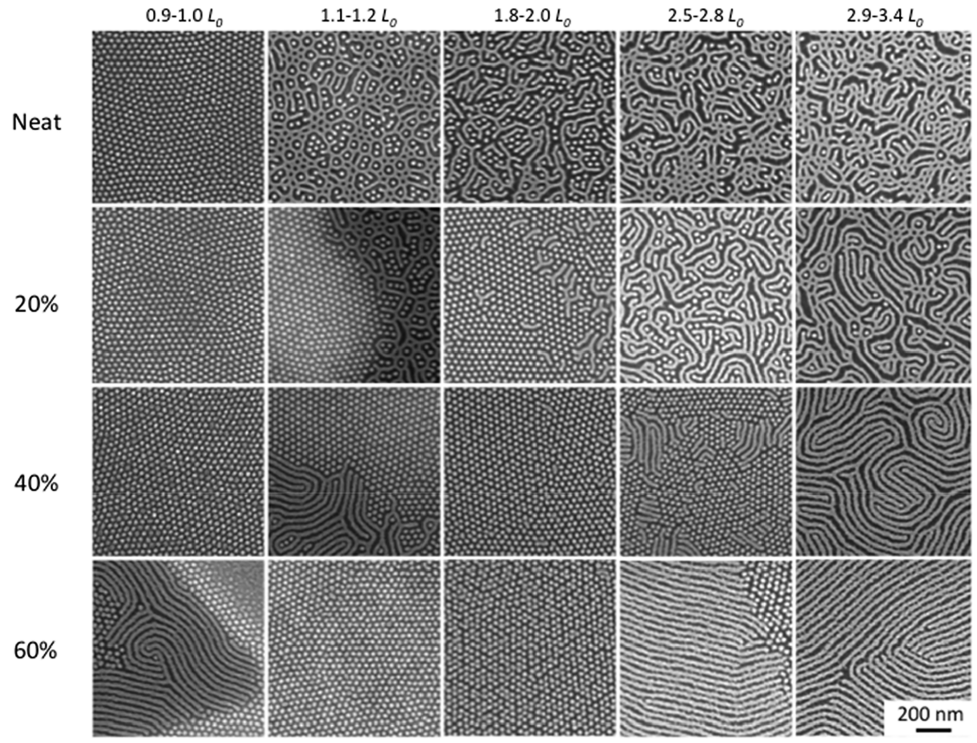

Figure 3. Plan-view SEMs of self-assembled cylinders in neat BCP and BCP/homopolymer ternary blend films after annealing at 200 °C for 1 h. Film thicknesses (in L_0 units) are indicated on the abscissa while homopolymer mass fractions are indicated on the ordinate. All images are at the same magnification.

relaxation mechanism is applicable in both scenarios. We conjecture that the different geometries of the two domain morphologies are the underlying origin for the different behavior. Critically, the arrangement of circular cylinder domains into a hexagonal lattice to most efficiently fill space introduces packing frustration, which is not present in the lamellae case. In the interstices between cylinders within the matrix phase (here PS), the PS block of the BCP chain must deform to fill space; added homopolymer, however, can fill the voids, allowing the BCP chain to relax.[29] This localization of the PS matrix homopolymer reduces its translational entropy and so competes with its tendency toward uniform distribution. It may even slightly reduce the PS homopolymer concentration near the domain interface, promoting asymmetric swelling of the cylinder domains that could in turn produce an overall contraction in domain spacing as a result of increased interfacial area per chain, similar to what has been observed for binary blends of a lamellar polystyrene-*block*-polyisoprene (PS-*b*-PI) BCP with low molecular weight PS homopolymer.[30] In the ternary lamellar blends studied in our previous work,[20] the contraction due to increased area per BCP chain is apparently offset by equivalent swelling of both blocks with homopolymer. Future experimental and computational work will be directed toward investigating this hypothesis.

The long-range order of the cylinder domain structure can be quantified by the average grain size (ξ) within which a uniform hexagonal lattice spatially persists. In GISAXS, ξ can be determined *in situ* during annealing based on a Scherrer-type analysis of the first-order scattering peak width.[23] Values of ξ measured during annealing at 200 and 220 °C for the neat BCP and blends containing 20% and 40% homopolymer are plotted as a function of time on a dual logarithmic scale in Figures 2c and 2d, respectively. Grain coarsening leads to an increase in ξ over the annealing time as described by a power law, $\xi = At^{\nu}$, where A is a prefactor encompassing various determinants of the overall scale of the ordering kinetics, such as its temperature dependence. The magnitude of the exponent ν, commonly termed the growth exponent, can provide insight into the mechanism for coarsening.[31] Consistent with the SEMs in Figure 1, the final values of ξ in Figure 2c indicate an overall level of order that is not substantially different between the blends and the neat BCP.

Straight lines in Figures 2c and 2d are power law fits to the experimental data. As shown in Figure 2c, the ordering exponent decreases slightly with increasing homopolymer mass fraction at 200 °C, yet values of ν are still generally comparable. All three are lower than ordering exponents previously measured for vertically oriented cylinder-forming PS-*b*-PMMA.[13,17] However, those measurements were based on image analysis of samples much greater than $1L_0$ thick that were annealed for long times; direct comparison with the samples analyzed *in situ* by GISAXS reported here is therefore difficult. In contrast to what is observed regarding the ordering exponent, the prefactor increases proportionally to homopolymer mass fraction. The diffusivity of polymer melts can be associated with "free volume" within the melt, correlated empirically through a logarithmic dependence on the difference between the annealing temperature and the glass transition temperature (T_g) (or a suitable reference temperature above T_g).[32,33] Because blending in small molecular weight homopolymer reduces the effective T_g of the blends with respect to the neat BCP, the blends can be viewed as ordering similarly to the neat BCP but at an effectively higher temperature, thus increasing the power law prefactor.

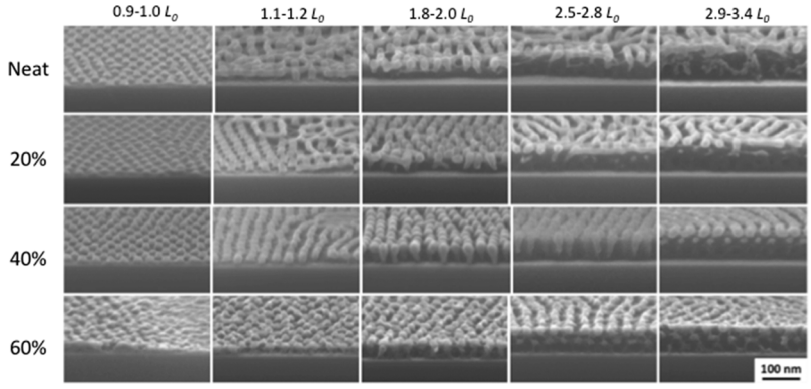

Figure 4. Cross-section SEMs of self-assembled cylinders in neat BCP and BCP/homopolymer ternary blend films after annealing at 200 °C for 1 h. Film thicknesses (in L_0 units) are indicated on the abscissa while homopolymer mass fractions are indicated on the ordinate. All images are at the same magnification.

The trends in A and ν are more dramatic for the samples annealed at 220 °C (Figure 2d). While the blend with a 20% homopolymer fraction shows an anomalously flat power law, the fits to the blends generally indicate a higher A and a lower ν compared to the neat BCP. As will be discussed later, this trend in the coarsening behavior of blends with vertically oriented cylinders becomes even more dramatic in thicker films.

Morphology and Orientation in Thicker Films. To gain a better understanding of the impact of thickness on the self-assembly behavior for neat and blend films, we created samples with multiple well-defined thicknesses for each blend by blade coating (see the Experimental Section) so that all thicknesses could be characterized *in situ* using GISAXS under the same annealing conditions. Afterward, the samples were infiltrated with Al_2O_3, partially etched with O_2 plasma treatment for enhanced contrast, and imaged by SEM. The overall effect of film thickness on the morphology and domain orientation of neat and blend films annealed at 200 °C is given by plan-view and cross-section SEMs in Figures 3 and 4, respectively (plan-view SEMs for films annealed at 220 °C are presented in Figure S4, while cross-section SEMs for the neat and 40% homopolymer blend annealed at 220 °C are presented in Figure S5). Film thicknesses (in L_0 units) are indicated on the abscissas while homopolymer mass fractions are indicated on the ordinates.

As noted previously, in films $<1L_0$ thick, vertically oriented cylinders are obtained for all compositions with <60% homopolymer, while dewetting occurs at a 60% homopolymer composition. However, once the film is more than $1L_0$ thick, the neat BCP does not self-assemble into a hexagonally ordered domain morphology with a consistent orientation during the annealing interval. Cross-section images indicate that the domains in the thicker neat films orient randomly across the thickness of the films. Note that infiltration of the Al_2O_3 does not penetrate to the bottom of the thickest films, preventing identification of the domain morphology or orientation at the substrate interface for those cases. The film thicknesses investigated here conform to a regime in which the topological ordering is dominated by interactions with the substrate interface or which features competition between substrate and free surface controlled ordering.[13,15] This competition may frustrate the development of well-oriented cylinders on the time scale of 1 h of annealing. Moreover, though cylindrical domains in films $<1L_0$ thick are energetically constrained to orient vertically, in thicker films there is ample opportunity during the ramp to the annealing temperature for the formation of disorganized, randomly oriented cylinder domains via microphase separation from the nominally disordered as-cast state. The combined effect of competition between substrate and free surface orientation control and the random initial orientation of cylindrical domains frustrates the ordering process for the neat BCP films with thicknesses $>1L_0$ investigated here.

Ordering is improved in the 20% homopolymer blend. At $\sim 1.1L_0$ thickness there is a coexistence of ordered vertically oriented cylinder with the frustrated morphology. At the $\sim 1.9L_0$ thickness, the fraction of vertically oriented cylinders is higher though it is clear from the SEM cross section that the cylinder domains do not orient vertically all the way to the substrate. For the thickest films, the 20% homopolymer blend morphology is only a little more developed than for the neat BCP. At a 40% homopolymer mass fraction, the film is dominated by hexagonally ordered cylindrical domains. For instance, while there is a coexistence of horizontal and vertical cylinders for $\sim 1.2L_0$ and $\sim 2.6L_0$ thick films, the areas with each orientation are clearly ordered. Cross-section SEMs in Figure 4 indicate that the hexagonally arranged cylinder morphologies extend toward the substrate, though the incomplete Al_2O_3 infiltration for the thickest film makes it impossible to determine if there is a third layer of cylinders nearest the substrate that follows the same hexagonal arrangement as the top two layers. At a 60% homopolymer mass fraction, either horizontal or vertical cylinder orientation tends to dominate for a particular film thickness, while the degree of topological order is noticeably improved across all film thicknesses, indicative of faster ordering kinetics.

From inspection of the SEMs, a tentative description of the overall ordering process in films more than $1L_0$ thick emerges, characterized by intermediate states that have been previously highlighted by Majewski and Yager.[18] During the temperature ramp, disorganized cylindrical domains with randomly oriented axes form throughout the film as part of the initial phase separation process. Subsequently, grains containing hexagonally ordered cylindrical domains that are oriented either vertically or horizontally nucleate and grow at the expense of the metastable, disorganized regions. Coexisting grains with either vertical or horizontal cylinders may also be present at an intermediate ordering stage. Thinner films tend to be replete with vertical cylinders while thicker films conversely exhibit a

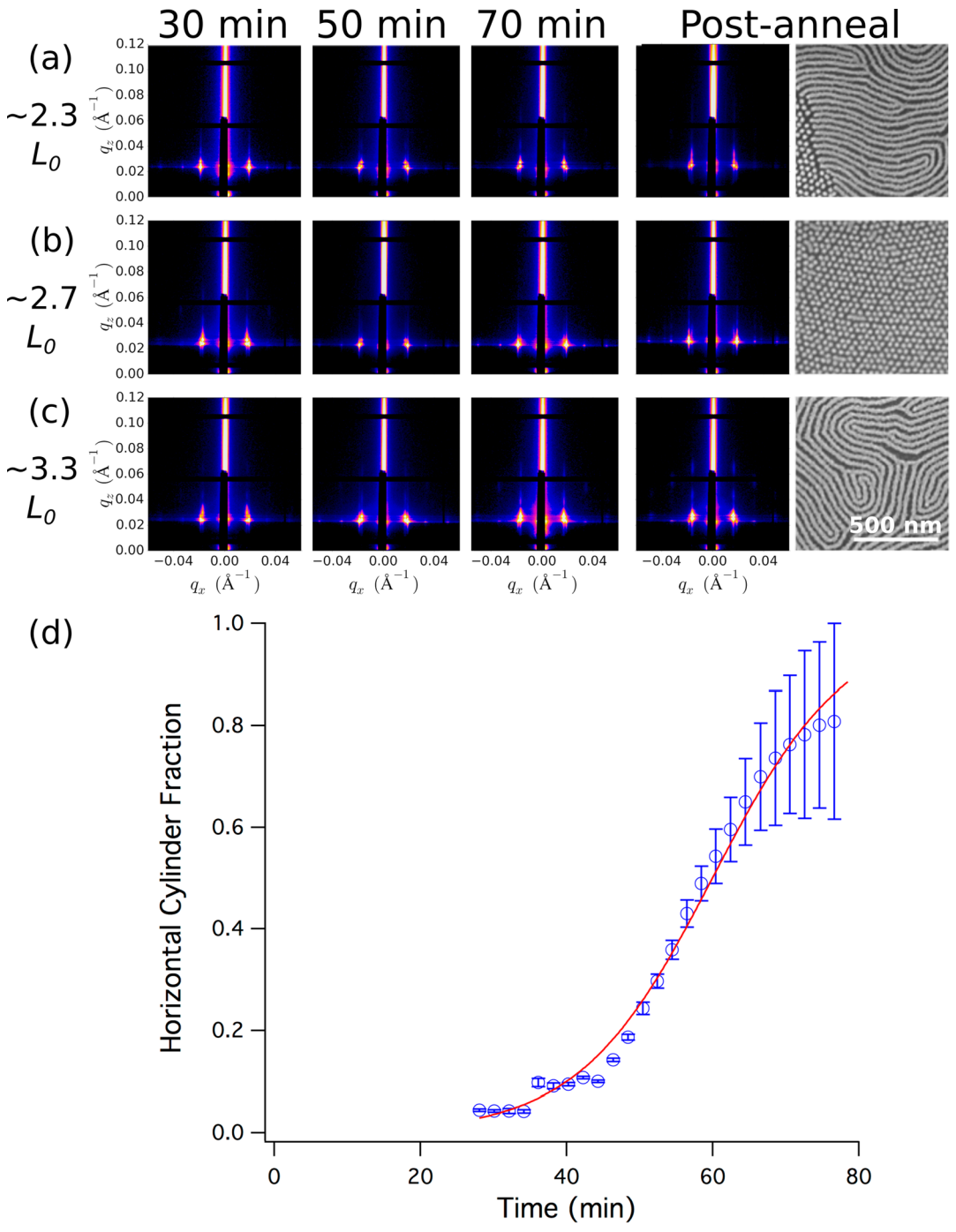

Figure 5. Cylinder domain reorientation in BCP/homopolymer ternary blend films with 40% homopolymer (w/w) annealed at 220 °C. (a–c) *In situ* GISAXS scattering images and postannealing, *ex situ* GISAXS scattering images and SEMs for films with thicknesses of (a) ~2.3L_0, (b) ~2.7L_0, and (c) ~3.3L_0. All SEMs are at the same magnification. (d) Estimated horizontal cylinder fraction during annealing for the ~2.3L_0 thick film in (a). The solid red line is a sigmoidal fit to the data according to eq 1.

preference for horizontal cylinders. This behavior may be attributed to the stronger role of the substrate surface in determining domain orientation in thinner films. In light of this description of the overall ordering process, the phases observed for the different blend compositions reflect the enhanced ordering kinetics afforded by ternary blends featuring small molecular weight homopolymers.

In situ GISAXS measurements indicate that coexisting vertical and horizontal cylinders observed for blend films at some film thicknesses are not stable, but instead represent quenched states during a reorientation transition. In the system investigated here, the ensuing orientation of cylinders depends on the film thickness. Representative GISAXS images for several thicknesses of a 40% homopolymer blend during annealing at 220 °C are shown in Figure 5. At 30 min for the ~2.3L_0 thick film (Figure 5a) there is a clear peak along the q_x direction that can be attributed to vertically oriented cylinders. The presence of higher-order scattering peaks along q_x indicates that the cylinders have formed a well-ordered hexagonally packed lattice rather than being randomly packed.

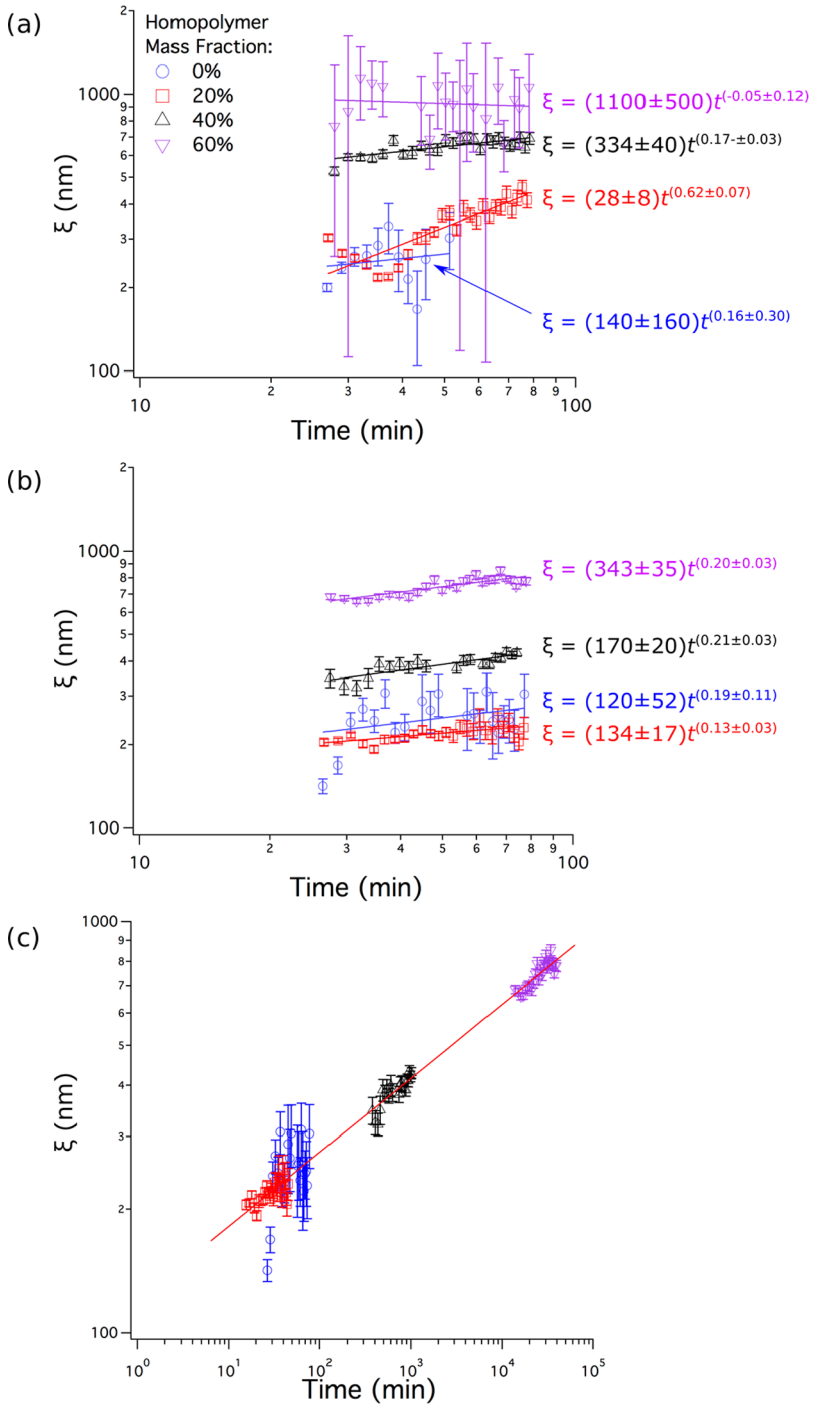

Figure 6. *In situ* GISAXS ordering measurements for neat and ternary blend films more than one monolayer thick during thermal annealing at 200 °C. Correlation length (ξ) as a function of annealing time for (a) 1.8−2.0L_0 and (b) 2.9−3.4L_0 thick films. Solid lines in (a) and (b) are power law fits to the data. (c) Plot of ξ in (b) where the time axis for data from the 20%, 40%, and 60% (w/w) blends have been multiplied by experimentally derived shift factors (a) to fall on a "master curve" using the neat BCP data as a reference. The solid red line is the interpolated master curve. The legend in (a) applies to all plots.

As annealing proceeds, however, a second nearby scattering peak emerges at a smaller q_x position but higher q_z position, pointing to the emergence of horizontally oriented cylinders. As annealing proceeds further, the horizontal-cylinder scattering peak grows in intensity while the vertical-cylinder peak decreases, consistent with a reorientation transition. Nevertheless, a coexisting vertical and horizontal cylinder population exists even after annealing.

Reorientation transitions also happen for other thicknesses in the same sample. For the ~2.7L_0 thick film (Figure 5b), two peaks are initially present and the horizontal cylinder orientation (smaller q_x) dominates, but over the course of annealing the vertical cylinder orientation overtakes it, resulting in a near-absence of horizontal cylinders after annealing, as shown by the postannealing SEM and GISAXS image at the far right. For the ~3.3L_0 thick film (Figure 5c), peaks for horizontal and vertical cylinders are also present

initially, but as annealing proceeds the horizontal cylinder peak grows in intensity while the vertical cylinder peak diminishes. Higher-order reflections along the q_z direction also emerge due to the presence of multiple horizontal cylinder layers within the film. The postanneal data show that the film has become completely composed of horizontally oriented cylinders. The tendency for films to reorient toward vertical or horizontal cylinders is clearly thickness dependent, though it may also depend on other factors that dictate the surface and substrate interfacial energies of the BCP thin film like annealing temperature and substrate treatment.

Analysis of the GISAXS spectra enables monitoring the relative fraction of horizontal (or vertical) cylinders in the film (see the Experimental Section) during annealing. This provides a way to determine the rate of reorientation transitions in the blend films. Calculated horizontal cylinder fractions for the $\sim 2.3L_0$ thick 40% homopolymer blend film annealed at 220 °C are shown in Figure 5d. The data for the fraction of horizontal cylinders (f_h) are fitted to a sigmoidal function of time (t) of the form

$$f_h = \frac{1}{1 + e^{-k_r(t-t_h)}} \quad (1)$$

where t_h is the time at which $f_h = 0.5$, and k_r is a reorientation rate constant. Fitting yields a value for k_r of 6.6 ± 0.2 h^{-1}. This is at least 1 order of magnitude faster than the rate constant for reorientation at 220 °C measured for neat films by Majewski and Yager,[18] again illustrating the enhancement in BCP self-assembly kinetics afforded by homopolymer blending.

It is also worth noting that in blends with a 60% homopolymer mass fraction the polymer can diffuse rapidly enough to generate micrometer-scale island/hole structures in films that are $\sim 3L_0$ or thicker, which predominantly self-assemble into horizontally oriented cylinders (see Figure S6 for examples). Such micrometer-scale polymer reorganization modulates the local thickness to accommodate an integer number of cylinder layers, thereby reducing entropic energy penalties associated with incommensurability between the film thickness and the cylindrical lattice spacing.[27] The rapidity in which this happens for the 60% homopolymer blends may play a critical role in dictating the dominant cylinder orientation for thicker films in this homopolymer composition range.

Ordering Kinetics in Thicker Films. To gain a better understanding of the ordering kinetics in BCP−homopolymer blends thicker than a monolayer, we employ the same correlation length measurement method based on *in situ* GISAXS discussed earlier with respect to sub-L_0 thick films. Beyond composition, the ordering kinetics can be a function of film thickness, temperature, and cylinder orientation;[31] therefore, we focus on samples annealed at 200 °C and minimal film thickness ranges in which the BCP−homopolymer blends exhibit the same nominal cylinder orientation. These conditions correspond to vertical cylinders at a film thickness of $1.8-2.0L_0$ and horizontal cylinders at a film thickness of $2.9-3.4L_0$ (columns 3 and 5, respectively, in Figures 3 and 4). Similar results are found in the samples annealed at 220 °C, but overall analysis is complicated by lack of conformity with respect to cylinder orientation within a film thickness range, especially when compounded with the phenomenon of cylinder reorientation transitions.

Figure 6a shows the time dependence of topological grain size across the blend compositions for vertical cylinders. The neat sample experienced a loss of signal intensity during annealing, likely due to misalignment, prohibiting accurate measurement beyond ~50 min. This results in a high error in its power law fit. For the blends, as the homopolymer mass fraction is increased from 20% to 60%, the power law prefactor increases by over ~3800%. At the same time, the ordering exponent ν decreases from ~0.6 to ~0 (within experimental error). On the other hand, the time dependence of topological grain size across the blend compositions for horizontal cylinders is starkly different (Figure 6b). In this case the measured ξ values are comparable between the neat and 20% homopolymer blend. Otherwise, the data in general show a consistent trend: a substantial increase in the prefactor A as the homopolymer mass fraction is increased, while ν maintains similar values across the range of compositions.

For the vertical cylinders, only the 40% homopolymer blend exhibits an exponent ν of ~0.17 that is reasonably consistent with previous reported ν values ranging from 0.14 to 0.29 for vertical cylinders from PS-*b*-PMMA block copolymers of similar molecular weight.[13−15,34] It should be noted that correlation lengths obtained by GISAXS analysis represent a sampling throughout the film and over large areas, which may diverge from SEM-extracted correlation lengths, especially when the ordering at the top surface of the BCP film is decoupled from the remainder of the film. Vertical cylinder ordering for the 20% homopolymer blend proceeds very rapidly ($\nu \approx 0.62$) from an initial state with poor order. However, examination of the corresponding SEM (Figure 3, row 2, column 3) shows that defective, horizontally oriented structures remain present at the boundaries of the vertical cylinder grains. In contrast to the behavior of the 20% homopolymer blend, the prefactor for the 60% homopolymer blend is much higher (by a factor of ~39 times that of the 20% homopolymer blend), but grain coarsening is nearly arrested within experimental error ($\nu \sim 0$).

Previous investigations of cylindrical BCP ordering have suggested an initial period of more rapid grain growth,[13,14] that slows once hexagonal order has developed and may even cease at late stages as grain boundaries are pinned.[35] Glasner[36] has recently highlighted these ordering regimes through simulations based on a dynamical model of hexagonal pattern coarsening. At early stages, coarsening dominated by defect annihilation gives rise to an $\sim t^{0.51}$ power law; at an intermediate stage an $\sim t^{0.23}$ power law is observed based on grain boundary migration and consumption of smaller grains; and at late stages the correlation length ceases to increase due to grain boundary pinning. Translated to homopolymer composition, these regimes appear to mirror the ordering behavior for vertical cylinders observed in the BCP/homopolymer blends. Following this analogy, the rapid ordering in the 20% homopolymer blend represents early stage coarsening based on localized defect annihilation. On the other hand, the 60% homopolymer blend has already coarsened to a late stage with $\nu \approx 0$ by the time isothermal measurements have commenced.

Power law fits of the grain size versus time for BCP−homopolymer blends self-assembling to horizontally oriented cylinders in Figure 6b exhibit a general ordering exponent in the vicinity of ~0.13−0.21, consistent with previous reports of the coarsening in horizontal BCP cylinder patterns.[17,37−39] However, the prefactor increases noticeably with increasing homopolymer mass fraction. The consistent ordering exponent values imply a self-similar behavior by which curves may be rigidly shifted in time to form a "master curve" based on

superposition. This practice of creating a master curve has been used to investigate the kinetics of BCP ordering as a function of temperature (relative to a reference temperature) based on the principle of time−temperature superposition.[37,40] Because the measurements performed here are isothermal, the resultant curve shifts reflect a "time−composition superposition", analogous to time−temperature superposition, indicating how increasing homopolymer fractions enhances the rate of ordering similarly to the way increasing temperature does. Curves shifted according to their mean ξ values using the prefactor fitted to the neat BCP data as the reference and an average ordering exponent of 0.18 are depicted in Figure 6c, along with the calculated power law master curve using these two parameters. This master curve visually indicates the time required to achieve the levels of order observed in the blends with a higher homopolymer fraction (40% and 60%) assuming they all have the same ordering exponent, which is approximately true. It is clear by inspection that the large increases in the value of A associated with blends with higher homopolymer mass fractions require time shifts exceeding an order of magnitude for all the data to fall on the same curve.

Though semiempirical in derivation, the Williams−Landel−Ferry (WLF) equation has been successfully used to capture the time−temperature superposition in block copolymer pattern coarsening based on the free volume theory:[37]

$$\log(a_{\mathrm{WLF}}) = \frac{17.44(T - T_{\mathrm{g}})}{51.6 + (T - T_{\mathrm{g}})} \tag{2}$$

The WLF equation must be based on a reference temperature, here chosen as T_{g}, where the equation is valid in the range of ~100 K above T_{g}[41] (our annealing temperatures are near this limit). Based on DSC measurements of the homopolymer,[20] a 20% increase in homopolymer mass fraction reduces the T_{g} for a blend by ~6−7 °C, thus increasing the relative temperature difference in the WLF equation. This permits conversion between time−temperature superposition and time−composition superposition through which appropriate shift factors based on free volume diffusivity enhancement can be estimated. These shift factors (a_{WLF}) are provided alongside the experimentally extracted values for horizontal cylinder ordering at a thickness of 2.9−3.4L_0, in Table 1. Though a_{WLF} is only slightly higher than the experimentally derived shift factor for the 20% blend, it is apparent that the WLF estimate does not adequately account for the experimentally observed kinetic enhancement of blending at higher homopolymer mass fractions.

Table 1. Experimental and Calculated Shift Factors

homopolymer mass fraction (%)	exptl shift factor (a)[a]	a_{WLF}[b]	$a_{\chi N}$[c]	$a_{\mathrm{combined}} = a_{\mathrm{WLF}}a_{\chi N}$
20	0.6 + 0.5/−0.3	1.8	4	7
40	14 + 9/−5	3	14	40
60	500 + 300/−200	5	50	240

[a]Error based on the ~95% confidence interval (2σ) of $\log(a)$. [b]Shift factors calculated according to eq 2. [c]Shift factors calculated according to eq 4.

Aside from the effect of free volume on polymer diffusivity, diffusion in BCPs is substantially hindered due to the excess energy required to pull the polymer from the minority block through the other domain or matrix,[42,43] specifically to pull PMMA through the PS matrix for the system studied here. Because this energetic barrier vanishes in the disordered state where no domains are present, the hindrance to BCP chain diffusion can be described by[43]

$$\frac{D}{D_{\mathrm{dis}}} = \mathrm{e}^{-\alpha(\chi N_{\mathrm{MMA}} - (\chi N_{\mathrm{MMA}})_{\mathrm{ODT}})} \tag{3}$$

where D is the polymer chain diffusion coefficient, D_{dis} is the diffusion coefficient in the disordered state, χ is the Flory−Huggins interaction coefficient between PS and PMMA, N_{MMA} is the degree of polymerization for the PMMA block, and α is a parameter of unity order. The "ODT" subscript indicates the value of the PMMA block segregation strength (χN_{MMA}) at which the BCP or blend undergoes an order−disorder transition. While blending small molecular weight PMMA and PS homopolymer with the BCP does not change χ, the more uniform homopolymer distribution within the self-assembled domains increases the fraction of small chains at domain interfaces, thereby decreasing interfacial tension between self-assembled domains and increasing the domain interface width.[44] As a result, when the blended homopolymers are small enough that they do not phase separate on their own, which is the case in this report, then increasing the homopolymer fraction in the blend brings the system closer to an order−disorder transition.[20] This reduces the difference term that comprises the energy barrier to polymer chain diffusion across domain interfaces presented in eq 3. While we did not observe an ODT directly in this work, as noted previously a significant reduction in topological order is observed when the homopolymer mass fraction is increased to 80% (Figure S2). This indicates that homopolymer blending indeed brings the system closer to an order−disorder transition.

We can estimate the magnitude of shift factors attributable to a reduction in segregation strength induced by homopolymer blending through the following equation (see the Supporting Information for the derivation):

$$\log(a_{\chi N}) = 0.434\alpha f_{\mathrm{MMA}}\chi\phi_{\mathrm{H}}(N - N_{\mathrm{H}}) \tag{4}$$

In this equation, f_{MMA} is the volume fraction of MMA block in the BCP, ϕ_{H} is the volume fraction of the homopolymer in the blend, N_{H} is the average degree of polymerization of the homopolymers, and 0.434 is the (truncated) base 10 logarithm of e. Because the homopolymer is added in the same mass proportion as the two blocks of the BCP, ϕ_{H} is effectively identical to the homopolymer mass fraction. Based on the polymers employed in the experiment, and assuming $\alpha = 1$, values of $f_{\mathrm{MMA}} = 0.29$, $N = 652$, $N_{\mathrm{H}} = 32$, and $\chi = 0.036$ at 200 °C (estimated based on a previously determined function of temperature[45]) were used to calculate shift factors based in eq 4 ($a_{\chi N}$). These calculated shift factors are included in Table 1, along with shift factors estimating the combined effect of segregation strength and free volume contributions ($a_{\mathrm{combined}} = a_{\mathrm{WLF}}a_{\chi N}$). No single set of calculated values matches experimental data very well; however, this may be expected since this heuristic approach to analysis excludes key factors like the interfacial width, the actual distribution of homopolymer within the melt, and any effects of entanglement, which would require a far more refined analysis. Nevertheless, it is clear that the impact of homopolymer blending on the effective segregation strength must be accounted for to explain the experimentally observed ordering kinetic enhancement.

Though the homopolymers used in this work are limited to a molecular weight of ∼3 kg/mol, it is expected that ordering kinetics could be enhanced even more if using smaller molecular weight homopolymers, or oligomers. First, blends featuring even lower molecular weight homopolymers will exhibit a lower effective T_g, leading to enhanced diffusivity based on free volume considerations. Second, lower molecular weight homopolymers may accumulate to a higher fraction at the domain interface and may even penetrate into the opposing domain, thereby decreasing the interfacial tension as well as the energy barrier hindering diffusion in self-assembled BCP films. However, this may also impose a faster transition to a disordered phase, in turn limiting the extent to which the smaller molecular weight homopolymer may be blended with the BCP.

Besides the physical aspects that influence the magnitude of the power law prefactor A described in the preceding paragraphs, it is important to note that its magnitude also reflects ordering dynamics prior to the initiation of measurements.[38] This suggests that the early stage ordering behavior (prior to isothermal GISAXS measurements) is critical to the enhanced prefactor observed in blends for both vertically and horizontally oriented cylinders. Given the substantial increase in A with increasing homopolymer mass fraction, contrasted with ordering exponents that are nominally similar for horizontal cylinders across the range of homopolymer mass fractions, the role of blending in this system can be thought of as rapid initial ordering that "jumps" toward a much later stage of the conventional coarsening process. For instance, a BCP film blended with 60% homopolymer rapidly (<3 min) orders to a state that would require >200 days of conventional annealing of an unblended film. Figure 7 shows SEMs of early stage morphologies in a 60% homopolymer mass fraction blend film annealed in a vacuum oven at 200 °C with thicknesses of ∼1.7L_0 and ∼2.9L_0, corresponding to vertical and horizontal cylinders, respectively. Images taken after 60 min of vacuum oven annealing are shown as a reference. Based on these images, a plausible description of early stage ordering can be developed: Initially, rapid phase separation engenders disorganized cylindrical domains with random orientations. Grains of both vertical and horizontal cylinders nucleate and compete with each other, where the lower energy (more stable) orientation depends on the film thickness and surface chemistry. Eventually, the more stable orientation dominates and grain growth follows mechanisms that have been outlined previously.[31,37] Vertical cylinder patterns appear to coarsen faster than horizontal cylinder ones, as evidenced by the fact that the ∼2.9L_0 thick sample annealed in a vacuum oven for 60 min still contains isolated vertical cylinder grains, though it is unclear from the present data whether that is a consequence of the cylinder orientation or is due to the lower thickness of the vertically oriented cylinder film. Under this description of early stage ordering, reorientation kinetics play a critical role in the coarsening process, where the enhanced diffusivity afforded through blending has a dramatic effect as shown earlier. Therefore, it is expected that strategies that promote particular cylinder orientations such as templating,[46,47] thermal gradients,[16,17,48] or shear[49−52] can be applied to blends to constructively enhance the ordering kinetics for desired patterns.

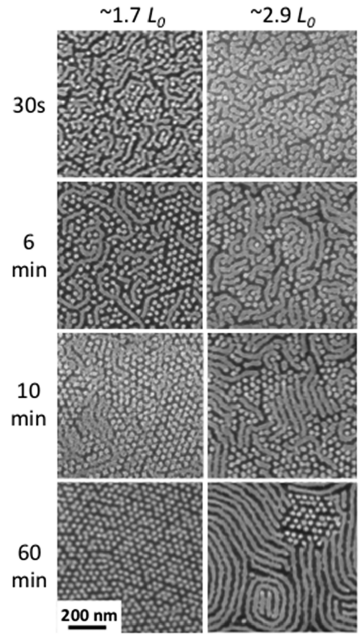

Figure 7. Plan-view SEMs of self-assembled cylinders in ∼1.7L_0 and ∼2.9L_0 thick BCP/homopolymer ternary blend films with a 60% homopolymer mass fraction after vacuum oven annealing at 200 °C for 30 s, 6 min, 10 min, or 60 min. All images are at the same magnification.

CONCLUSIONS

In summary, we have investigated self-assembly kinetics and domain orientation in films of varying thickness comprising a PS-*b*-PMMA BCP blended with low molecular weight PS and PMMA homopolymer (∼3 kg/mol) in proportions that retain the cylindrical morphology of the neat (unblended) BCP. *In situ* GISAXS and *ex situ* SEM imaging were used to uncover key aspects of the ordering process. Above ∼1 cylinder monolayer thickness, self-assembled ordering is frustrated in neat films, whereas ordered cylinder patterns coarsen in blends with a rate that generally increases in proportion to the homopolymer mass fraction. Ternary blending with small molecular weight homopolymers substantially enhances the rate of transitions between horizontal and vertical cylinder orientations, having a direct effect on early stage ordering in which there is competition between the two orientations. However, once patterns with clear hexagonal symmetry fully develop, the enhancement to coarsening kinetics granted by homopolymer blending is minimal. These intriguing results highlight the importance of kinetically controlled, pathway-dependent ordering in the formation of self-assembled BCP patterns.

AUTHOR INFORMATION

Corresponding Author

*E-mail: gdoerk@bnl.gov.

ORCID

Gregory S. Doerk: 0000-0002-2933-2047

Kevin G. Yager: 0000-0001-7745-2513

Present Address

A.R.: Mechanical Engineering Department, Cornell University, Ithaca, NY 14853.

Notes

The authors declare no competing financial interest.

■ ACKNOWLEDGMENTS

This research was carried out at the Center for Functional Nanomaterials and the National Synchrotron Light Source II, Brookhaven National Laboratory, which are supported by the U.S. Department of Energy (DOE) Office of Science under Contract DE-SC0012704.

■ REFERENCES

(1) Doerk, G. S.; Yager, K. G. Beyond Native Block Copolymer Morphologies. *Mol. Syst. Des. Eng.* **2017**, *2* (5), 518−538.

(2) Ruiz, R.; Kang, H.; Detcheverry, F. A.; Dobisz, E.; Kercher, D. S.; Albrecht, T. R.; de Pablo, J. J.; Nealey, P. F. Density Multiplication and Improved Lithography by Directed Block Copolymer Assembly. *Science* **2008**, *321* (5891), 936−939.

(3) Checco, A.; Rahman, A.; Black, C. T. Robust Superhydrophobicity in Large-Area Nanostructured Surfaces Defined by Block-Copolymer Self Assembly. *Adv. Mater.* **2014**, *26* (6), 886−891.

(4) Rahman, A.; Ashraf, A.; Xin, H.; Tong, X.; Sutter, P.; Eisaman, M. D.; Black, C. T. Sub-50-nm Self-Assembled Nanotextures for Enhanced Broadband Antireflection in Silicon Solar Cells. *Nat. Commun.* **2015**, *6*, 5963.

(5) Liapis, A. C.; Rahman, A.; Black, C. T. Self-Assembled Nanotextures Impart Broadband Transparency to Glass Windows and Solar Cell Encapsulants. *Appl. Phys. Lett.* **2017**, *111* (18), 183901.

(6) Gopinadhan, M.; Deshmukh, P.; Choo, Y.; Majewski, P. W.; Bakajin, O.; Elimelech, M.; Kasi, R. M.; Osuji, C. O. Thermally Switchable Aligned Nanopores by Magnetic-Field Directed Self-Assembly of Block Copolymers. *Adv. Mater.* **2014**, *26* (30), 5148−5154.

(7) Peinemann, K.-V.; Abetz, V.; Simon, P. F. W. Asymmetric Superstructure Formed in a Block Copolymer via Phase Separation. *Nat. Mater.* **2007**, *6* (12), 992−996.

(8) Zhou, C.; Segal-Peretz, T.; Oruc, M. E.; Suh, H. S.; Wu, G.; Nealey, P. F. Fabrication of Nanoporous Alumina Ultrafiltration Membrane with Tunable Pore Size Using Block Copolymer Templates. *Adv. Funct. Mater.* **2017**, *27* (34), 1701756.

(9) Black, C. T.; Ruiz, R.; Breyta, G.; Cheng, J. Y.; Colburn, M. E.; Guarini, K. W.; Kim, H.-C.; Zhang, Y. Polymer Self Assembly in Semiconductor Microelectronics. *IBM J. Res. Dev.* **2007**, *51* (5), 605−633.

(10) Ham, S.; Shin, C.; Kim, E.; Ryu, D. Y.; Jeong, U.; Russell, T. P.; Hawker, C. J. Microdomain Orientation of PS- *b* -PMMA by Controlled Interfacial Interactions. *Macromolecules* **2008**, *41* (17), 6431−6437.

(11) Han, E.; Stuen, K. O.; La, Y.-H.; Nealey, P. F.; Gopalan, P. Effect of Composition of Substrate-Modifying Random Copolymers on the Orientation of Symmetric and Asymmetric Diblock Copolymer Domains. *Macromolecules* **2008**, *41* (23), 9090−9097.

(12) Han, E.; Stuen, K. O.; Leolukman, M.; Liu, C.-C.; Nealey, P. F.; Gopalan, P. Perpendicular Orientation of Domains in Cylinder-Forming Block Copolymer Thick Films by Controlled Interfacial Interactions. *Macromolecules* **2009**, *42* (13), 4896−4901.

(13) Ji, S.; Liu, C.-C.; Liao, W.; Fenske, A. L.; Craig, G. S. W.; Nealey, P. F. Domain Orientation and Grain Coarsening in Cylinder-Forming Poly(Styrene- *b* -Methyl Methacrylate) Films. *Macromolecules* **2011**, *44* (11), 4291−4300.

(14) Ferrarese Lupi, F.; Giammaria, T. J.; Volpe, F. G.; Lotto, F.; Seguini, G.; Pivac, B.; Laus, M.; Perego, M. High Aspect Ratio PS- *b* -PMMA Block Copolymer Masks for Lithographic Applications. *ACS Appl. Mater. Interfaces* **2014**, *6* (23), 21389−21396.

(15) Ferrarese Lupi, F.; Giammaria, T. J.; Seguini, G.; Laus, M.; Dubček, P.; Pivac, B.; Bernstorff, S.; Perego, M. GISAXS Analysis of the In-Depth Morphology of Thick PS- *b* -PMMA Films. *ACS Appl. Mater. Interfaces* **2017**, *9* (12), 11054−11063.

(16) Samant, S.; Strzalka, J.; Yager, K. G.; Kisslinger, K.; Grolman, D.; Basutkar, M.; Salunke, N.; Singh, G.; Berry, B.; Karim, A. Ordering Pathway of Block Copolymers under Dynamic Thermal Gradients Studied by *in Situ* GISAXS. *Macromolecules* **2016**, *49* (22), 8633−8642.

(17) Majewski, P. W.; Yager, K. G. Millisecond Ordering of Block Copolymer Films *via* Photothermal Gradients. *ACS Nano* **2015**, *9* (4), 3896−3906.

(18) Majewski, P. W.; Yager, K. G. Reordering Transitions during Annealing of Block Copolymer Cylinder Phases. *Soft Matter* **2016**, *12* (1), 281−294.

(19) Choo, Y.; Majewski, P. W.; Fukuto, M.; Osuji, C. O.; Yager, K. G. Pathway-Engineering for Highly-Aligned Block Copolymer Arrays. *Nanoscale* **2018**, *10* (1), 416−427.

(20) Doerk, G. S.; Yager, K. G. Rapid Ordering in "Wet Brush" Block Copolymer/Homopolymer Ternary Blends. *ACS Nano* **2017**, *11* (12), 12326−12336.

(21) Vaselabadi, S. A.; Shakarisaz, D.; Ruchhoeft, P.; Strzalka, J.; Stein, G. E. Radiation Damage in Polymer Films from Grazing-Incidence X-Ray Scattering Measurements. *J. Polym. Sci., Part B: Polym. Phys.* **2016**, *54* (11), 1074−1086.

(22) SciAnalysis; https://github.com/CFN-softbio/SciAnalysis (accessed July 31, 2018).

(23) Smilgies, D.-M. IUCr. Scherrer Grain-Size Analysis Adapted to Grazing-Incidence Scattering with Area Detectors. *J. Appl. Crystallogr.* **2009**, *42* (6), 1030−1034.

(24) Bai, W.; Yager, K. G.; Ross, C. A. *In Situ* Characterization of the Self-Assembly of a Polystyrene−Polydimethylsiloxane Block Copolymer during Solvent Vapor Annealing. *Macromolecules* **2015**, *48* (23), 8574−8584.

(25) Peng, Q.; Tseng, Y.-C.; Darling, S. B.; Elam, J. W. A Route to Nanoscopic Materials via Sequential Infiltration Synthesis on Block Copolymer Templates. *ACS Nano* **2011**, *5* (6), 4600−4606.

(26) Kamcev, J.; Germack, D. S.; Nykypanchuk, D.; Grubbs, R. B.; Nam, C.-Y.; Black, C. T. Chemically Enhancing Block Copolymers for Block-Selective Synthesis of Self-Assembled Metal Oxide Nanostructures. *ACS Nano* **2013**, *7* (1), 339−346.

(27) Black, C. T.; Forrey, C.; Yager, K. G. Thickness-Dependence of Block Copolymer Coarsening Kinetics. *Soft Matter* **2017**, *13* (18), 3275−3283.

(28) Stuen, K. O.; Thomas, C. S.; Liu, G.; Ferrier, N.; Nealey, P. F. Dimensional Scaling of Cylinders in Thin Films of Block Copolymer−Homopolymer Ternary Blends. *Macromolecules* **2009**, *42* (14), 5139−5145.

(29) Matsen, M. W. Phase Behavior of Block Copolymer/Homopolymer Blends. *Macromolecules* **1995**, *28* (17), 5765−5773.

(30) Winey, K. I.; Thomas, E. L.; Fetters, L. J. Swelling of Lamellar Diblock Copolymer by Homopolymer: Influences of Homopolymer Concentration and Molecular Weight. *Macromolecules* **1991**, *24* (23), 6182−6188.

(31) Majewski, P. W.; Yager, K. G. Rapid Ordering of Block Copolymer Thin Films. *J. Phys.: Condens. Matter* **2016**, *28* (40), 403002.

(32) Milhaupt, J. M.; Lodge, T. P.; Smith, S. D.; Hamersky, M. W. Composition and Temperature Dependence of Monomer Friction in Polystyrene/Poly(Methyl Methacrylate) Matrices. *Macromolecules* **2001**, *34* (16), 5561−5570.

(33) Tong, Q.; Sibener, S. J. Visualization of Individual Defect Mobility and Annihilation within Cylinder-Forming Diblock Copolymer Thin Films on Nanopatterned Substrates. *Macromolecules* **2013**, *46* (21), 8538−8544.

(34) Seguini, G.; Zanenga, F.; Laus, M.; Perego, M. Ordering Kinetics in Two-Dimensional Hexagonal Pattern of Cylinder-Forming PS- b -PMMA Block Copolymer Thin Films: Dependence on the Segregation Strength. *Phys. Rev. Mater.* **2018**, *2* (5), 055605.

(35) Boyer, D.; Viñals, J. Weakly Nonlinear Theory of Grain Boundary Motion in Patterns with Crystalline Symmetry. *Phys. Rev. Lett.* **2002**, *89* (5), 055501.
(36) Glasner, K. Hexagonal Phase Ordering in Strongly Segregated Copolymer Films. *Phys. Rev. E* **2015**, *92* (4), 042602.
(37) Harrison, C.; Cheng, Z.; Sethuraman, S.; Huse, D. A.; Chaikin, P. M.; Vega, D. A.; Sebastian, J. M.; Register, R. A.; Adamson, D. H. Dynamics of Pattern Coarsening in a Two-Dimensional Smectic System. *Phys. Rev. E: Stat. Phys., Plasmas, Fluids, Relat. Interdiscip. Top.* **2002**, *66* (1), 011706.
(38) Ruiz, R.; Bosworth, J. K.; Black, C. T. Effect of Structural Anisotropy on the Coarsening Kinetics of Diblock Copolymer Striped Patterns. *Phys. Rev. B: Condens. Matter Mater. Phys.* **2008**, *77* (5), 054204.
(39) Giammaria, T. J.; Ferrarese Lupi, F.; Seguini, G.; Perego, M.; Vita, F.; Francescangeli, O.; Wenning, B.; Ober, C. K.; Sparnacci, K.; Antonioli, D.; et al. Micrometer-Scale Ordering of Silicon-Containing Block Copolymer Thin Films via High-Temperature *T*hermal Treatments. *ACS Appl. Mater. Interfaces* **2016**, *8* (15), 9897−9908.
(40) Ceresoli, M.; Volpe, F. G.; Seguini, G.; Antonioli, D.; Gianotti, V.; Sparnacci, K.; Laus, M.; Perego, M. Scaling of Correlation Length in Lamellae Forming PS-b-PMMA Thin Films upon High Temperature Rapid Thermal Treatments. *J. Mater. Chem. C* **2015**, *3* (33), 8618−8624.
(41) Williams, M. L.; Landel, R. F.; Ferry, J. D. The Temperature Dependence of Relaxation Mechanisms in Amorphous Polymers and Other Glass-Forming Liquids. *J. Am. Chem. Soc.* **1955**, *77* (14), 3701−3707.
(42) Cavicchi, K. A.; Lodge, T. P. Self-Diffusion and Tracer Diffusion in Sphere-Forming Block Copolymers. *Macromolecules* **2003**, *36* (19), 7158−7164.
(43) Yokoyama, H. Diffusion of Block Copolymers. *Mater. Sci. Eng., R* **2006**, *53* (5−6), 199−248.
(44) Broseta, D.; Fredrickson, G. H.; Helfand, E.; Leibler, L. Molecular Weight and Polydispersity Effects at Polymer-Polymer Interfaces. *Macromolecules* **1990**, *23* (1), 132−139.
(45) Russell, T. P.; Hjelm, R. P.; Seeger, P. A. Temperature Dependence of the Interaction Parameter of Polystyrene and Poly(Methyl Methacrylate). *Macromolecules* **1990**, *23* (3), 890−893.
(46) Ji, S.; Liu, C.-C.; Liu, G.; Nealey, P. F. Molecular Transfer Printing Using Block Copolymers. *ACS Nano* **2010**, *4* (2), 599−609.
(47) Rahman, A.; Majewski, P. W.; Doerk, G.; Black, C. T.; Yager, K. G. Non-Native Three-Dimensional Block Copolymer Morphologies. *Nat. Commun.* **2016**, *7*, 13988.
(48) Singh, G.; Yager, K. G.; Smilgies, D.-M.; Kulkarni, M. M.; Bucknall, D. G.; Karim, A. Tuning Molecular Relaxation for Vertical Orientation in Cylindrical Block Copolymer Films via Sharp Dynamic Zone Annealing. *Macromolecules* **2012**, *45* (17), 7107−7117.
(49) Majewski, P. W.; Rahman, A.; Black, C. T.; Yager, K. G. Arbitrary Lattice Symmetries via Block Copolymer Nanomeshes. *Nat. Commun.* **2015**, *6*, 7448.
(50) Majewski, P. W.; Yager, K. G. Block Copolymer Response to Photothermal Stress Fields. *Macromolecules* **2015**, *48* (13), 4591−4598.
(51) Majewski, P. W.; Yager, K. G. Latent Alignment in Pathway-Dependent Ordering of Block Copolymer Thin Films. *Nano Lett.* **2015**, *15* (8), 5221−5228.
(52) Angelescu, D. E.; Waller, J. H.; Adamson, D. H.; Deshpande, P.; Chou, S. Y.; Register, R. A.; Chaikin, P. M. Macroscopic Orientation of Block Copolymer Cylinders in Single-Layer Films by Shearing. *Adv. Mater.* **2004**, *16* (19), 1736−1740.